Characteristic length scale for strain fields around impurity cations in perovskites

Michael A. Carpenter and Ruth E. A. McKnight
Department of Earth Sciences, University of Cambridge, Downing Street, Cambridge CB2 3EQ, United Kingdom

Christopher J. Howard
Department of Earth Sciences, University of Cambridge, Downing Street, Cambridge CB2 3EQ, United Kingdom and School of Engineering, University of Newcastle, New South Wales 2308, Australia

Qingdi Zhou and Brendan J. Kennedy
School of Chemistry, The University of Sydney, New South Wales 2006, Australia

Kevin S. Knight
ISIS Facility, Rutherford Appleton Laboratory, Chilton, Didcot, Oxfordshire OX11 0QX, United Kingdom
(Received 20 April 2009; revised manuscript received 26 October 2009; published 2 December 2009)

Lattice parameters have been determined from high-resolution neutron-powder diffraction data collected as a function of temperature for perovskites in the $Pr_{1-x}La_xAlO_3$ solid solution in order to determine the influence of La doping on the $Imma \leftrightarrow C2/m$ transition temperature, T_c^*. A plateau in T_c^* at ~150 K extends to $x \approx 0.016 \pm 0.002$, followed by a linear reduction with increasing $LaAlO_3$ content. The plateau is interpreted in terms of a saturation effect such that there is a composition limit below which the strain fields surrounding individual La^{3+} ions are isolated in the $PrAlO_3$ matrix and above which they overlap. On this basis the strain fields are estimated to have diameters of ~16–18 Å, which appears to be a characteristic length scale for structural relaxation around dopant atoms and other types of local clusters in oxide perovskites.

DOI: 10.1103/PhysRevB.80.214101 PACS number(s): 64.70.kp, 61.50.Ks, 61.05.fm

I. INTRODUCTION

Strain fields which develop by structural relaxation around impurity atoms substituted into a crystal have fundamental implications for the structure, properties, and behavior of solid solutions. For perovskites they must play an important part in determining the extent to which local distortions, in relaxors, ferroelectric or Jahn-Teller systems for example, correlate favorably to give long-range order or unfavorably to give rise to frustration. Even small strain effects can induce dramatic changes in electronic structure and physical properties, as elegantly demonstrated by Ahn and Millis[1] for the substrate-induced strain in thin-film perovskites. Their influence is manifest also in other, unexpected behavior. For example, in $(Ca,Sr)TiO_3$ perovskites octahedral tilting transitions occur with substantially reduced spontaneous strains at intermediate compositions, as if the local strains are responsible for suppression of strain/order parameter coupling without changing the evolution of the order parameter itself.[2] In this case, indirect evidence of the length scale of the local strain fields is given by line broadening in powder absorption IR spectra.[3] This view is reinforced by the behavior of $La_{0.6}Sr_{0.1}TiO_3$, in which strain/order parameter coupling for a tilting transition can be switched on and off by altering the extent of cation order on the *A* sites.[4] Another example is the pseudocubic lattice geometry which is observed for the high-temperature forms of $La_xCa_{1-x}MnO_3$.[5] In this case it is likely that frustration effects of overlapping strain fields around disordered Mn^{3+} and Mn^{4+} suppress the macroscopic distortions from orthorhombic lattice geometry.[6] Cation disordering has also been observed to suppress magnetoresistance effects in manganites.[7] Other related examples of the same phenomenon abound in perovskites such as the well known relaxor behavior of $SrTiO_3$ once a small proportion of Sr is replaced by Ca (e.g., Refs. 8 and 9).

Local strain behavior is likely to be a significant factor, if not the dominant factor, when minor impurities are introduced into perovskites. The length scale of such strain fields will determine the width of a plateau region of transition temperature for second-order displacive transitions in dilute solid solutions. In the present study the primary objective was to make use of this effect, for the $Imma \leftrightarrow C2/m$ transition in $Pr_{1-x}La_xAlO_3$, to determine the effective dimension of local strain fields around La^{3+} substituted for Pr^{3+}. Although a specific system has been chosen, the scientific question is generic. Doping of perovskites with impurity atoms is a common practice for controlling, modifying or creating advantageous physical properties, and it is the wider issue of the local scale mechanism for these effects, rather than the specifics of the system $Pr_{1-x}La_xAlO_3$ alone that are at issue.

The basis of the plateau effect is that the transition temperature, T_c, of some second-order displacive phase transition in a chemically pure crystal is likely to be the same as in a crystal with only one atom replaced by an impurity atom. The impurity atom will be surrounded by a local strain field, however, and as additional substitutions are made, these will eventually overlap. Once the strain fields overlap, T_c will deviate from that of the pure phase and will start to increase or decrease with further substitution. The width of the plateau of constant T_c is thus an indirect indication of the effective size of individual strain fields.[10–17] In the mineral albite, $NaAlSi_3O_8$, which has a three-dimensional framework structure, a plateau in T_c for the $C2/m \leftrightarrow C\bar{1}$ transition extends to ~2 mol. % $KAlSi_3O_8$, which means that the strain fields around each K^+ replacing Na^+ must be 20–40 Å in

diameter.[15,16] The same transition has a plateau extending to ~10 mol. % $CaAl_2Si_2O_8$ in the plagioclase feldspar solid solution, implying strain fields around Ca^{2+} of $\leq \sim 20$ Å in diameter. A plateau width of ~12% $ZnWO_4$ in $CuWO_4$ implies strain fields of ~8 Å around Zn^{2+} (Ref. 18) and ~10%Mg component at a pressure driven transition in the chain silicate cummingtonite $(Fe,Mg)_7Si_8O_{22}(OH)_2$ implies a strain field diameter of ~5–10 Å around Mg^{2+}.[19] Romero *et al.*[20] have suggested ~30 Å strain fields around Ca^{2+} in $KMnF_3$ but this is based on limited data. Salje[11] used transition temperatures for the $PbZr_xTi_{1-x}O_3$ solid solution to suggest that the $Pm\bar{3}m \leftrightarrow P4mm$ transition has a plateau extending out to $x \approx 0.03$. This transition is first order in character in the pure end member but tricritical at $x \approx 0.06$,[21] however, indicating that the influence of strain is more complicated than simply renormalizing the critical temperature, T_c. In particular, changes in the strain/order parameter coupling coefficient can renormalize the fourth-order coefficient in the excess free energy and so change the thermodynamic character from first order to second order. Ca-doped $KMnF_3$ also shows this pattern of behavior. It is necessary to choose a second-order transition to isolate the influence of strain fields on the transition temperature alone.

Of all the displacive phase transitions in perovskites that were known to the present authors, the $Imma \leftrightarrow C2/m$ transition in $(Pr,La)AlO_3$ appeared to offer the best combination of features which might allow the determination of a small plateau region to high precision. In particular, the transition is pseudoproper ferroelastic in character and gives rise to deviations from $\beta=90°$ which can be followed with a high degree of precision by neutron-powder diffraction on the high resolution powder diffractometer at ISIS. The transition occurs at ~150 K in pure $PrAlO_3$ (Refs. 22–30) and the full phase diagram is given in Fig. 1 (making use of data from Glynn *et al.*[31] and Kennedy *et al.*).[32] The octahedral tilting transition, $Pm\bar{3}m \leftrightarrow R\bar{3}c$, is at sufficiently high temperatures that it does not have a direct influence on the $Imma \leftrightarrow C2/m$ transition, which is considered to be driven primarily by cooperative Jahn-Teller distortions of the Pr coordination polyhedron. The $R\bar{3}c \leftrightarrow Imma$ transition can be understood as occurring as a consequence of strain coupling between the tilting and Jahn-Teller transitions,[29] and is not considered further here.

II. SPONTANEOUS STRAIN

For the purpose simply of following the $Imma \leftrightarrow C2/m$ transition temperature as a function of composition, it is not necessary to consider the full Landau expansion with coupled Jahn-Teller and octahedral tilting order parameters developed by Carpenter *et al.*[29] The $C2/m$ structure is more conveniently described in terms of an $I2/m$ cell which has the same orientation as the *Imma* cell. Coupling of the strain with a single-order parameter is then given by[33]

$$G = \frac{1}{2}a\Theta_s\left[\coth\left(\frac{\Theta_s}{T}\right) - \coth\left(\frac{\Theta_s}{T_c}\right)\right]Q^2 + \frac{1}{4}bQ^4 + (\lambda_1 e_1 + \lambda_2 e_2 + \lambda_3 e_3)Q^2 + \lambda_5 e_5 Q + (\lambda_4 e_4^2 + \lambda_6 e_6^2)Q^2 + \lambda_7 e_4 e_6 Q + \frac{1}{2}\sum_{i=1-6} C_{ii}^o e_i^2 + \frac{1}{2}\sum_{i,k=1-3} C_{ik}^o e_i e_k, \quad (1)$$

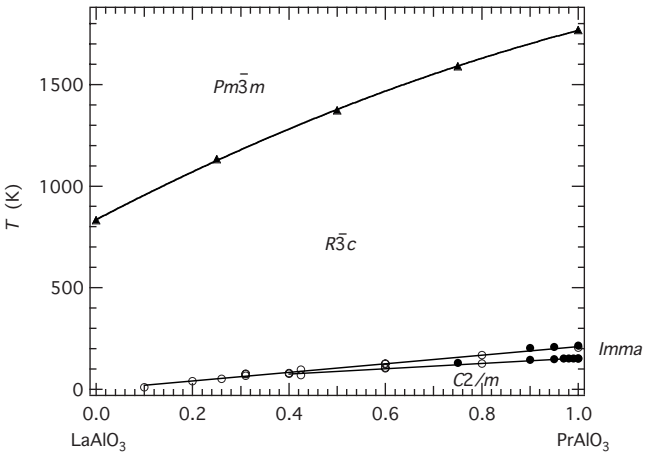

FIG. 1. Subsolidus phase diagram for the $Pr_{1-x}La_xAlO_3$ solid solution. Filled triangles are transition temperatures for the $Pm\bar{3}m \leftrightarrow R\bar{3}c$ transition taken from Kennedy *et al.* (Ref. 32). Open circles represent transition temperatures delineating stability fields of *Imma* and $C2/m$ structures taken from Glynn *et al.* (Ref. 31). Filled circles are transition temperatures from Carpenter *et al.* (Ref. 29) and this study. Glynn *et al.* (Ref. 31) described the $C2/m$ structure as being triclinic, but it is assumed here that the monoclinic structure is the stable phase at low temperatures almost across to pure $LaAlO_3$.

where Q is the order parameter, Θ_s is the order-parameter saturation temperature, e_i are components of the spontaneous strain, λ_i are coupling coefficients, and C_{ik}^o are elastic constants of the parent *Imma* structure. The reference system to which the spontaneous strains refer has X, Y, and Z parallel to crystallographic x, y, and z axes. For a second-order transition the order-parameter and symmetry-breaking strain e_5 are expected to evolve as

$$Q^2 = \left(\frac{C_{55}^o}{\lambda_5}\right)^2 e_5^2 = \frac{a\Theta_s}{b^*}\left[\coth\left(\frac{\Theta_s}{T_c^*}\right) - \coth\left(\frac{\Theta_s}{T}\right)\right]. \quad (2)$$

T_c^* is the transition temperature renormalized in the usual way by the bilinear coupling term, $\lambda_5 e_5 Q$, and b^* is the fourth order coefficient renormalized by the linear-quadratic coupling terms, $\lambda_i e_i Q^2$ $(i=1-3)$. The symmetry-breaking strain is given by[33]

$$e_5 = \frac{c}{c_o}\cos\beta \approx \cos\beta, \quad (3)$$

where c_o is the lattice parameter of the *Imma* phase extrapolated into the stability field of the $I2/m$ phase and c, β are lattice parameters of the $I2/m$ phase.

III. EXPERIMENTAL DETAILS

Lattice parameter data were obtained from two separate sets of samples during three different visits to the ISIS neutron facility, Rutherford Appleton Laboratories. Six of the first set of samples, Pr_{100}, Pr_{99}, Pr_{98}, Pr_{97}, Pr_{95}, and Pr_{90}, were prepared from Pr_6O_{11}, La_2O_3, and $Al(NO_3)_3.9H_2O$. For the seventh sample, Pr_{75}, Al_2O_3 was used instead of

$Al(NO_3)_3.9H_2O$. The sequence of mixing, grinding and firing at high temperatures used for the synthesis has been described by Carpenter *et al.*[29] Al_2O_3 was present as a residual impurity, and the Pr_{75} sample also gave broader powder diffraction peaks than the others. The second set of samples, with the same compositions, was prepared subsequently by first preheating Pr_6O_{11} and La_2O_3 overnight at 1000 °C. These were mixed with Al_2O_3 and fired at 1200 °C for 30 h, 1300 °C/65 h, 1400 °C/65 h, and 1450 °C/20 h, with grinding between each firing. Impurity phases in the final samples were estimated to be, from x-ray powder diffraction, <1 wt% Pr_2O_3 in Pr_{100}, Pr_{99}, Pr_{98}, Pr_{97}, Pr_{95}, Pr_{90}, and ~4 wt. % Al_2O_3+0.3 wt. % Pr_2O_3 in Pr_{75}. Approximately 20 or 50 mg of each sample was dissolved in concentrated nitric acid. The solutions were then diluted down so that the La:Pr ratios could be checked by ICPMS. These confirmed the nominal compositions to be correct, within experimental uncertainty. For example, two separate samples of Pr_{97} had measured Pr/(La+Pr) values (including some repeats) of 0.970, 0.968, and 0.972 while two Pr_{75} samples had measured values of 0.764, 0.773, 0.758, and 0.745.

Neutron-diffraction patterns were recorded using the high-resolution powder diffractometer (HRPD). The first set of samples was investigated during two separate sessions of beam time, Pr_{100}, Pr_{95}, and Pr_{90} in 2001 and Pr_{99}, Pr_{98}, Pr_{97}, and Pr_{75} in 2003. Data collection, results and a complete strain analysis for Pr_{100}, Pr_{95}, Pr_{90}, and Pr_{75} have already been published.[29] Data for Pr_{99}, Pr_{98}, and Pr_{97} from these earlier experiments were collected and analyzed in the same way but the results have not previously been reported. All seven of the second set of samples were investigated in a single three day experimental period during 2008. Aside from normal variations between samples associated with their synthesis such as crystallinity, grain size, and stoichiometry, it should be anticipated that there will be systematic differences between the three sets of data due to changes in thermocouple and other instrumental calibrations. Because the third data set was collected in a single beam time session, it would be expected to yield an internally consistent set of transition temperatures subject only to variations between samples arising from their synthesis.

Experimental details of data collection and sample environment conditions for the 2001 and 2003 data sets have been described by Carpenter *et al.*[29] In those experiments an AS Scientific, 50 mm diameter, "orange" helium cryostat, was used to establish temperature (monitored through a Rh/Fe sensor) and the exchange gas was He at 30 mbar. For the 2008 data set, ~13 gm of each sample was loaded into a 10-mm-thick aluminum slab can that also housed a heater and Rh/Fe sensor. The assembly was mounted on a center stick and then cooled in a Sumitomo 415 closed cycle refrigerator with 60–80 mbars of He exchange gas. Automatic data collection proceeded in a heating sequence starting at ~8 K, with 10 K steps at the lowest temperatures, 5 K steps at higher temperatures, and 2.5 K steps through T_c^*. A period of 5 min was allowed for thermal equilibration at each temperature. Diffraction patterns were recorded in the three detector banks over the time-of-flight range 30–130 ms, for a total incident proton beam of 8 μA h, corresponding to approximately 15 min, sufficient to give a good determination of lattice parameters. The immediate focus in this study being on lattice parameter determination, only the patterns from the high-resolution back-scattering detector banks were used. The patterns were normalized and corrected for detector efficiency according to prior calibration with a vanadium scan.

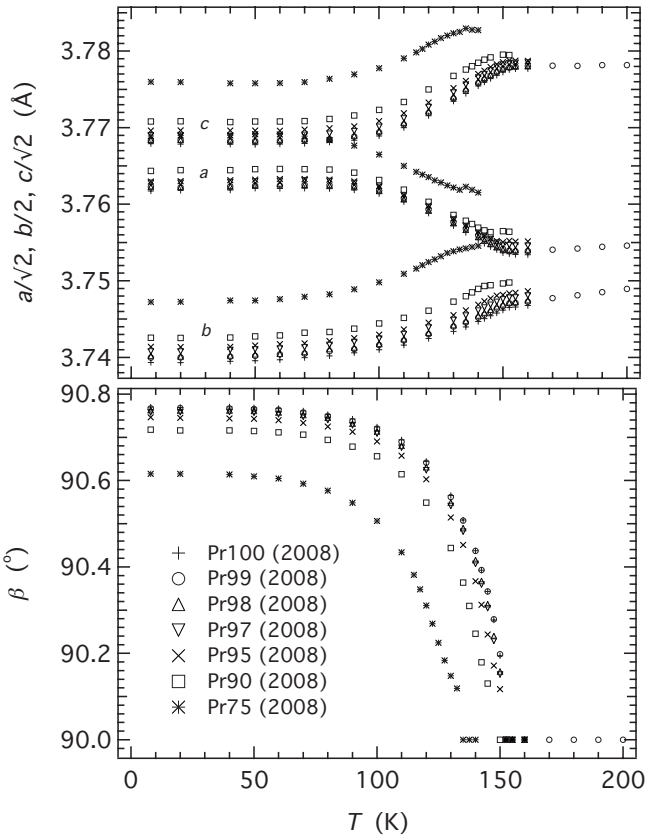

FIG. 2. Lattice parameter variations for the complete 2008 suite of samples.

Lattice parameters and atomic coordinates were refined from the diffraction patterns using the Rietveld method, as implemented in the GSAS computer program.[34] Peak shapes were modeled as convolutions of back-to-back exponentials with pseudo-Voigt functions in which two peak width parameters were varied, and the background as five-parameter shifted Chebyshev polynomials. Importantly, the diffractometer "constant" DIFA (Ref. 34) was determined once for each sample and not allowed to vary through the temperature series. Peak broadening of the 202 reflection from the *Imma* phase above T_c^* and of each of the $20\bar{2}/202$ doublet reflections below T_c^* was also followed by peak fitting in the manner of Carpenter *et al.*[29] The pseudo-Voigt function was used for the fitting, the widths in the $20\bar{2}/202$ doublet below the transition were constrained to be equal, and the results were compared with the width of the 040 peak, which should be unaffected.

IV. RESULTS

Lattice parameter data for the 2008 set of seven samples are given in Fig. 2. These show the same pattern of variation

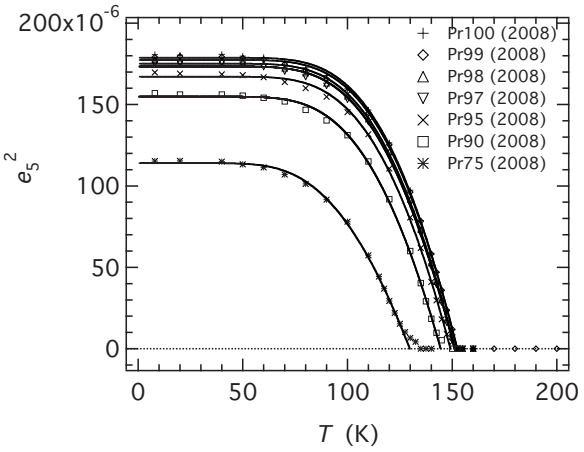

FIG. 3. Fitting of Eq. (4) to data for the 2008 suite, to obtain values of the $Imma \leftrightarrow C2/m$ transition temperature ($e_5^2 \approx \cos^2 \beta \propto Q^2$).

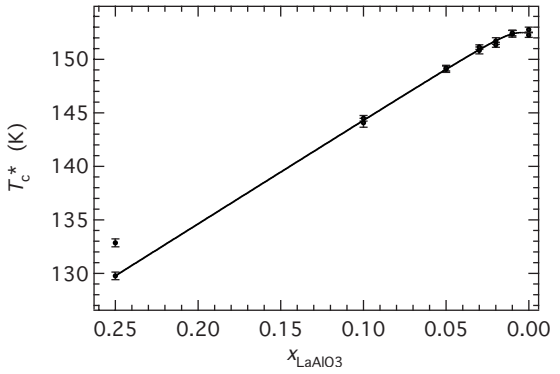

FIG. 4. Variation in T_c^* for the $Imma \leftrightarrow C2/m$ transition as a function of composition in the $Pr_{1-x}La_xAlO_3$ solid solution. The curve is a fit of Eq. (6) to the data, excluding the outlier at $x=0.25$.

as previously described for Pr_{100}.[29] At each composition b and c increase and a decreases continuously with increasing temperature through T_c^*. Similarly β goes continuously to 90° at $T=T_c^*$, within the experimental limits of resolution. The variation of $\cos^2 \beta$ is shown as a function of temperature in Fig. 3. Fits to the data according to

$$\cos^2 \beta = A\left[\coth\left(\frac{\Theta_s}{T_c^*}\right) - \coth\left(\frac{\Theta_s}{T}\right)\right], \quad (4)$$

achieved within the software package IGOR (Wavemetrics) are also shown and the resulting values of A, T_c^*, and Θ_s are given in Table I. To these have been added values for the same parameters obtained from sets of lattice parameters collected from the first set of samples. The temperature range of fitting was from the lowest measured temperature up to a few degrees below T_c^*. This procedure produced an internally consistent set of transition temperatures which avoided the tails near T_c^*, particularly evident in the data for Pr_{75} and Pr_{90}, that could be real consequences of defects and/or sample heterogeneity, or artifacts arising from fitting to peaks broadened by the usual influence of susceptibility at a pseudoproper ferroelastic transition.

TABLE I. Fit parameters extracted from high-resolution lattice parameter data for $Pr_{1-x}La_xAlO_3$.

Sample	T_c^* (K)	Θ_s (K)	$\frac{A}{\Theta_s} = \frac{a}{b^*}\left(\frac{\lambda_5}{C_{55}^o}\right)^2$ (K^{-1})	T_c^* rescaled (K)
Pr_{100} (2001)	151.26(24)	335.8(7.3)	0.0000213(26)	152.77(24)
Pr_{95} (2001)	147.62(30)	312.3(8.3)	0.0000174(17)	149.07(30)
Pr_{90} (2001)	142.55(42)	296.9(9.0)	0.0000158(16)	144.07(42)
Pr_{99} (2003)	148.79(33)	317.2(8.6)	0.0000172(26)	152.39(33)
Pr_{98} (2003)	148.10(31)	313.2(8.3)	0.0000176(25)	151.71(31)
Pr_{97} (2003)	147.23(32)	306.4(8.7)	0.0000171(26)	150.83(32)
Pr_{75} (2003)	129.25(37)	211.0(5.7)	0.0000046(6)	132.85(37)
Pr_{100} (2008)	152.26(22)	338.8(6.3)	0.0000223(23)	
Pr_{99} (2008)	152.45(25)	334.4(6.8)	0.0000211(24)	
Pr_{98} (2008)	151.35(23)	328.7(6.5)	0.0000203(22)	
Pr_{97} (2008)	151.13(22)	323.9(6.3)	0.0000192(20)	
Pr_{95} (2008)	149.17(27)	319.8(7.4)	0.0000188(24)	
Pr_{90} (2008)	144.49(27)	304.9(7.2)	0.0000170(22)	
Pr_{75} (2008)	129.76(36)	239.4(6.7)	0.0000093(1)	

Values of T_c^* are tightly constrained by the experimental data. There are systematic differences of up to ~4 K between the three sets of data, however, which are attributed to calibration changes for temperature or absolute lattice parameters between visits to ISIS. In order to produce a single, internally consistent set of values, T_c^* values from the second group, Pr_{99}, Pr_{98}, and Pr_{97} have been rescaled by the average difference between them and the samples with the same compositions from 2008 (3.60 K). The same adjustment was made to the observed value of T_c^* for Pr_{75} (2003). Values for the first group, Pr_{100}, Pr_{95}, and Pr_{90} (2001) have been similarly rescaled by the average difference between them and the 2008 values (1.47 K). These slight adjustments produce a tightly constrained, internally consistent set of transition temperatures from which only one sample deviates. Pr_{75} from the first set of samples had broader diffraction lines than the other samples and a higher level of Al_2O_3 impurity. The second Pr_{75} sample also had broader diffraction peaks and a slightly higher impurity content than the other samples, but had the advantage of being made by the same route and at the same time as the entire second set and is therefore marginally preferred. The final set of rescaled T_c^* values is listed in Table I and shown in Fig. 4. Values of Θ_s and A/Θ_s, ($\propto a\lambda_5^2/b^* C_{55}^{o2}$), without any rescaling, are shown in Fig. 5.

The full width at half maximum height of 040 and $20\bar{2}/202$ reflections showed the same pattern of evolution as given in Fig. 4 of Carpenter *et al.*[29] for Pr_{100}, with an increase in the widths of $20\bar{2}/202$ as the transition point was approached from either side. This is consistent with the expected behavior for a pseudoproper ferroelastic phase transition. All diffraction peaks were broader for Pr_{75} than for the other samples, but showed the same pattern of variation through T_c^*.

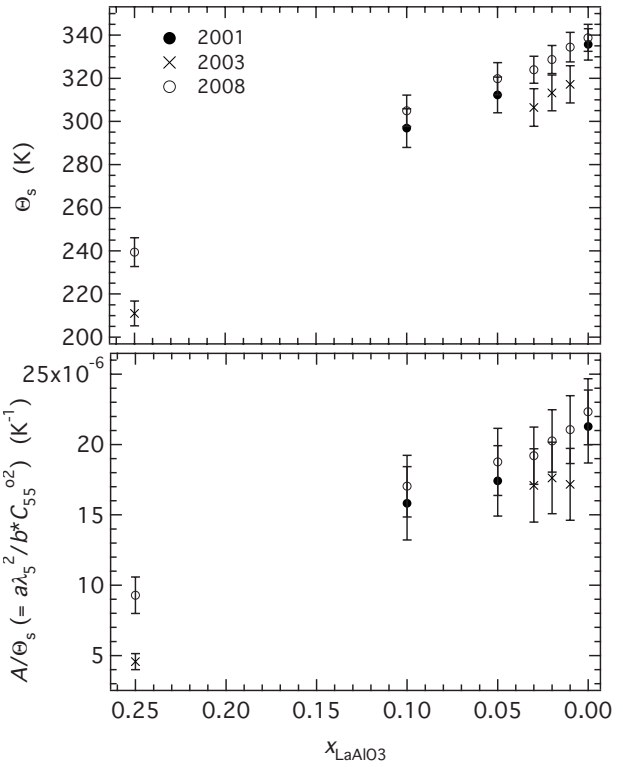

FIG. 5. Variations in Θ_s and A/Θ_s from fitting Eq. (4) to data for e_5^2 as a function of temperature.

V. DISCUSSION

The simplest view of the plateau effect is that impurity atoms behave as hard spheres inserted into spherical holes in an elastic matrix which are not quite the correct size for them. Strain dominates and the energy change depends on the difference in size between the sphere and the hole, together with the elastic properties of the matrix. The standard solution for strain around a spherical inclusion in an elastic medium has the magnitude of the strain, ε, decaying with distance, R, as $\varepsilon \propto R^{-3}$.[35] Observational evidence of long ranging strain fields of up to at least ~ 0.1 μm is provided by details of twin microstructures in feldspar minerals,[36] for example. On this basis the width of a plateau in T_c for a second-order transition away from a pure end member composition should be negligibly small. At the other extreme, an impurity atom might be accommodated by displacements of atoms only in its immediate coordination sphere, in which case the relaxation could not be described in terms of continuum elasticity. The strain field should have well defined limits and should give rise to a measurable plateau in T_c with a width which will depend primarily on the spacing between crystallographic sites on which the atomic substitution occurs. The fact that there is a measurable plateau for the $Imma \leftrightarrow C2/m$ transition in $Pr_{1-x}La_xAlO_3$ extending to $x \approx 0.01-0.02$ immediately implies that the effective strain field around La^{3+} is restricted to a few unit cells.

Salje[11] developed a generalized treatment of localized defects to show how variations in their character can lead to different forms of T_c variations with concentration. Of these, the most directly relevant had, as a starting point, coupling between impurity concentration, c, and the order parameter, Q, as proportional to cQ^2. Local regions around the impurity are considered to have a different transition temperature from the rest of the crystal and variations in T_c are obtained by treating the crystal as if it consists of two phases. There are two compositional ranges in which T_c varies linearly with composition, one at low impurity concentrations and the second at high concentrations within the solid solution, and there is a crossover between the two. The resulting variation is described by

$$T_c(x) = T_c(x=0) + m_1 x + (m_2 \pm m_1)x \tanh\left(\frac{x - x_p}{\Delta x}\right), \quad (5)$$

where x_p is the concentration at the crossover, $(2m_1 - m_2)$ is the slope dT_c/dx for the dilute limit, $x \to 0$, and m_2 is the slope for the solid solution. For a flat plateau $(2m_1 - m_2 = 0)$ this gives $T_c(x=0)$ as having the same value as would be obtained by extrapolation from the bulk of the solid solution, however, which is not generally the case. In the model used here, the character of the plateau is more akin to a saturation effect—there is some concentration below which changing composition no longer has any influence on the transition temperature of the whole crystal. By analogy with order parameter saturation at low temperatures, as incorporated in Eq. (1), we therefore make use of a coth function and describe the plateau using

$$T_c^*(x) = B_0 + B_1 \coth\frac{X_s}{x}, \quad (6)$$

where B_0 and B_1 are constants and X_s is an effective saturation composition. This follows the general treatment for the evolution of individual lattice parameters as $T \to 0$ K,[29,37–43] giving zero slope at $x \to 0$ and linear behavior away from the saturation regime. Equation (6) has been fit to the experimental data for T_c^* as a function of La^{3+} concentration in $PrAlO_3$, giving $B_0 = 154.1 \pm 0.2$ K, $B_1 = -1.6 \pm 0.3$ K, and $X_s = 0.016 \pm 0.002$ (mole fraction of $LaAlO_3$). $Pr_{75}(2003)$ was excluded from the fit on the basis that the sample gave relatively poor diffraction patterns and was therefore considered to be chemically inhomogeneous. The fit provides a good description of the remaining data (Fig. 4).

In order to relate the plateau width to a relaxation distance around individual La^{3+} ions, the coordination geometry of the cubic perovskite structure has been examined in terms of the spacings between dodecahedral sites and the numbers of such sites within each coordination sphere. There are six such sites at distance a from a given reference site, twelve at distance $\sqrt{2}a$, eight at distance $\sqrt{3}a$, etc., where a is the primitive cubic lattice parameter. If one in seven of the Pr^{3+} ions is replaced at random by La^{3+} $(x = 0.1429)$ and the radius of its strain field is $(1+\sqrt{2})a/2$, the strain fields around two adjacent La^{3+} ions would just impinge. Similarly the radius for impinging strain fields would become $(\sqrt{2} + \sqrt{3})a/2$ at $x = 0.0503$ (1 in 19), and so on for successive coordination spheres. This gives the relationship between the radius of impinging strain fields and concentration shown in Fig. 6, using $a = 3.75$ Å, which then represents the expected relationship for plateau width as a function of relaxation dis-

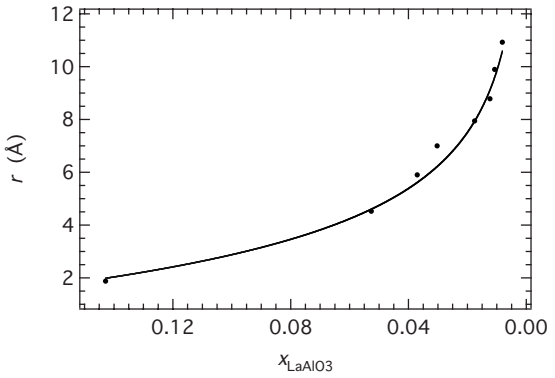

FIG. 6. Model for the variation in strain clouds around La^{3+} ions as a function of composition in $Pr_{1-x}La_xAlO_3$, with r representing the radius of strain clouds which just overlap at a given $LaAlO_3$ content, x. Data points are for successive coordination spheres of A cation sites round a single site. The curve is a power-law fit ($r = -15.5 + 13.3x^{-0.14}$ Å) for interpolation between data points.

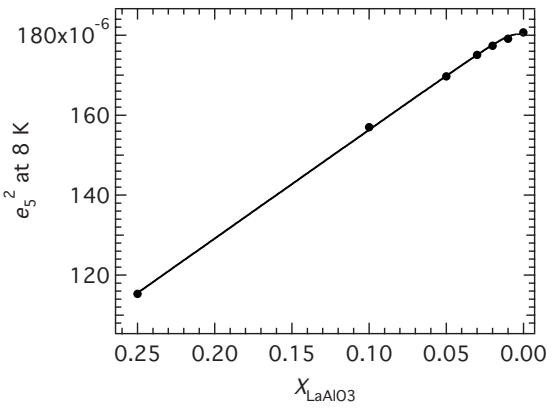

FIG. 7. Variation in e_5^2 ($\propto Q^2$) as a function of composition at 8 K for the 2008 suite of samples. For coupling between composition and the order parameter of the form λXQ^2, the variation in Q^2 is expected to show the same variation as T_c^*, as appears to be the case. The curve is a fit of Eq. (6) to all the data and has $X_s = 0.013 \pm 0.003$.

tance round each La^{3+} ion. A power law, $r = -15.5 + 13.3x^{-0.14}$ Å has been used to interpolate between points. On this basis, the value of X_s between ~0.018 and ~0.014 obtained from the fit to the T_c^* data implies strain fields which have radii in the range ~8–9 Å. Deviations from linearity only occur below $x = \sim 0.04$ at most, implying a minimum possible radius for the strain fields of ~5–6 Å.

Strain fields with radii ~8–9 Å (16–18 Å in diameter) correspond to effective relaxation distances around impurity atoms extending across ~2–3 unit cells. The same dimension has been reported for ferroelectric nanoscale domains within $SrSnO_3$ (10–15 Å diameter[44]), and ordered clusters of distorted MnO_6 octahedra above the Jahn-Teller cooperative ordering transition in $LaMnO_3$ (~16 Å).[45] Bednorz and Muller[8] identified $x = 0.016 \pm 0.002$ in $Sr_{1-x}Ca_xTiO_3$ as a critical composition for a change in dielectric properties with temperature, which corresponds exactly with the limiting composition for the change from isolated to overlapping strain clouds around La^{3+} in $Pr_{1-x}La_xAlO_3$. Clusters with a coherence length of ~20 Å have also been reported for manganite solid solutions,[46–48] and this coincidence would appear to suggest that the correlation length for any local structural perturbation in a perovskite is determined essentially by a strain relaxation mechanism. Whether the precise length scale is sensitive to the elastic constants remains to be seen but, to a first approximation, it is likely to be similar for most oxide perovskites. On this basis, impurity atoms and local cation disorder would be expected to have a major influence on phase separation in manganite solid solutions,[49] with implications for all the changes in electronic and magnetic properties which follow.

This empirical treatment of plateau behavior is consistent with the existence of local strain heterogeneities surrounding cations of different sizes in the perovskite structure. From an analysis of different spontaneous strains accompanying an improper ferroelastic transition in $La_{0.6}Sr_{0.1}TiO_3$ with ordered and disordered cation distributions, Howard *et al.*[4] concluded that such local strain heterogeneities can suppress the coupling of octahedral tilting with the macroscopic strain. This would be equivalent to reducing the values of the coupling coefficients $\lambda_1 - \lambda_3$ in Eq. (1), hence also reducing the value of the renormalized fourth order coefficient, b^*, in the normal manner (e.g., see Refs. 10 and 13). For phase transitions which are just first order in character ($b^* < 0$), an additional effect of the substitution of impurity ions with different radii into a pure end member phase should therefore be to change the character from first order to second order through a tricritical point, as occurs for Ca^{2+} substitution in $KMnF_3$,[20] Zr^{4+} substitution in $PbTiO_3$ (Ref. 21) and Ba^{2+} substitution in $LaMnO_3$.[6] There are insufficient data at high temperature to allow values of $\lambda_1 - \lambda_3$ to be determined from the present sets of data for $(Pr,La)AlO_3$, but the saturation temperature, Θ_s, and A/Θ_s, ($\propto a\lambda_5^2/b^*C_{55}^{o2}$) obtained from fitting e_5^2 display an approximately linear reduction with increasing La^{3+} content. A more complete description of the order parameter evolution could therefore be developed by allowing some composition dependence for the coefficients in Eq. (1). The view that mean-field behavior applies is supported by the composition dependence of the order parameter at constant temperature. This should reflect the variation of T_c^* if the order parameter couples with composition, X, as λXQ^2.[13,50,51] As expected, data for e_5^2 ($\propto Q^2$) at 8 K indeed show the same plateau as T_c^* (Fig. 7). Indirect evidence for the existence of heterogeneous strains on the same length scale in silicates and oxides more generally is provided by line broadening in powder infrared absorption spectra.[3,16,17,52–57]

In conclusion, a simple experiment on a carefully chosen phase transition using the highest possible resolution in strain to determine the composition dependence of T_c for a second-order transition appears to reveal a characteristic length scale for strain fields around impurity atoms in perovskites. The influence of the strain fields is likely to appear also in the thermodynamic character of the transition, in the mixing properties of perovskite solid solutions, including phase separation, and in field effects ahead of transition points. Their influence is most marked in the plateau region, however, and suggest that the high sensitivity of many materials properties to perturbations, as recently reviewed by

Millis,[58] could be addressed from the perspective of local strain relaxations over distances limited to a few unit cells.

ACKNOWLEDGMENTS

Support from the Leverhulme Foundation for C.J.H. and from the Australian Research Council (Grant No. DP0877695) is gratefully acknowledged. Travel for C.J.H. to ISIS in 2001 was provided by the Commonwealth of Australia through its Access to Major Research Facilities Program. The neutron facilities at ISIS are operated by the Science and Technology Facilities Council (STFC) with contributions from the Australian Institute of Nuclear Science Engineering and the Australian Research Council.

[1] K. H. Ahn and A. J. Millis, Phys. Rev. B **64**, 115103 (2001).
[2] M. A. Carpenter, C. J. Howard, K. S. Knight, and Z. Zhang, J. Phys.: Condens. Matter **18**, 10725 (2006).
[3] H.-W. Meyer, M. A. Carpenter, A. I. Becerro, and F. Seifert, Am. Mineral. **87**, 1291 (2002).
[4] C. J. Howard, Z. Zhang, M. A. Carpenter, and K. S. Knight, Phys. Rev. B **76**, 054108 (2007).
[5] X. G. Li, R. K. Zheng, G. Li, H. D. Zhou, R. X. Huang, J. Q. Xie, and Z. D. Wang, Europhys. Lett. **60**, 670 (2002).
[6] M. A. Carpenter and C. J. Howard, Acta Crystallogr. B **65**, 147 (2009).
[7] L. M. Rodriguez-Martinez and J. P. Attfield, Phys. Rev. B **54**, R15622 (1996).
[8] J. G. Bednorz and K. A. Müller, Phys. Rev. Lett. **52**, 2289 (1984).
[9] W. Kleemann, A. Albertini, M. Kuss, and R. Lindner, Ferroelectrics **203**, 57 (1997).
[10] E. K. H. Salje, *Phase Transitions in Ferroelastic and Co-Elastic Crystals* (Cambridge University Press, Cambridge, 1990).
[11] E. K. H. Salje, Eur. J. Mineral. **7**, 791 (1995).
[12] E. Salje, U. Bismayer, B. Wruck, and J. Hensler, Phase Transit. **35**, 61 (1991).
[13] M. A. Carpenter, in *The Stability of Minerals*, edited by G. D. Price and N. L. Ross (Chapman and Hall, London, 1992), p. 172.
[14] M. A. Carpenter, in *Energy Modelling in Minerals*, edited by C. M. Gramaccioli, EMU Notes in Mineralogy Vol. 4 (Eötvös University Press, Budapest, 2002), p. 311.
[15] S. A. Hayward and E. K. H. Salje, Am. Mineral. **81**, 1332 (1996).
[16] M. A. Carpenter, T. Boffa Ballaran, and A. J. Atkinson, Phase Transit. **69**, 95 (1999).
[17] M. A. Carpenter and T. Boffa Ballaran, in *Solid Solutions in Silicate and Oxide Systems*, edited by C. A. Geiger, EMU Notes in Mineralogy Vol. 3 (Eötvös University Press, Budapest, 2001), p. 155.
[18] S. A. T. Redfern and P. F. Schofield, Phase Transit. **59**, 25 (1996).
[19] T. Boffa Ballaran, R. J. Angel, and M. A. Carpenter, Eur. J. Mineral. **12**, 1195 (2000).
[20] F. J. Romero, M. C. Gallardo, S. A. Hayward, J. Jiménez, J. del Cerro, and E. K. H. Salje, J. Phys.: Condens. Matter **16**, 2879 (2004).
[21] R. W. Whatmore, R. Clarke, and A. M. Glazer, J. Phys. C **11**, 3089 (1978).
[22] R. D. Burbank, J. Appl. Crystallogr. **3**, 112 (1970).
[23] E. Cohen, M. D. Sturge, R. J. Birgeneau, E. I. Blount, L. G. Van Uitert, and J. K. Kjems, Phys. Rev. Lett. **32**, 232 (1974).
[24] M. D. Sturge, E. Cohen, L. G. Van Uitert, and R. P. Van Stapele, Phys. Rev. B **11**, 4768 (1975).
[25] K. B. Lyons, R. J. Birgeneau, E. I. Blount, and L. G. Van Uitert, Phys. Rev. B **11**, 891 (1975).
[26] R. J. Birgeneau, J. K. Kjems, G. Shirane, and L. G. Van Uitert, Phys. Rev. B **10**, 2512 (1974).
[27] R. T. Harley, W. Hayes, A. M. Perry, and S. R. P. Smith, J. Phys. C **6**, 2382 (1973).
[28] S. M. Moussa, B. J. Kennedy, B. A. Hunter, C. J. Howard, and T. Vogt, J. Phys.: Condens. Matter **13**, L203 (2001).
[29] M. A. Carpenter, C. J. Howard, B. J. Kennedy, and K. S. Knight, Phys. Rev. B **72**, 024118 (2005).
[30] S. Watanabe, M. Hidaka, H. Yoshizawa, and B. M. Wanklyn, Phys. Status Solidi B **243**, 424 (2006).
[31] T. J. Glynn, R. T. Harley, W. Hayes, A. J. Rushworth, and S. H. Smith, J. Phys. C **8**, L126 (1975).
[32] B. J. Kennedy, C. J. Howard, A. K. Prodjosantoso, and B. C. Chakoumakos, Appl. Phys. A: Mater. Sci. Process. **74**, s1660 (2002).
[33] M. A. Carpenter and E. K. H. Salje, Eur. J. Mineral. **10**, 693 (1998).
[34] A. C. Larson and R. B. Von Dreele, General Structure Analysis System (GSAS), Los Alamos National Laboratory Report No. LAUR 86–748, 2004 (unpublished).
[35] S. P. Timoshenko and J. N. Goodier, *Theory of Elasticity*, 3rd ed. (McGraw-Hill, New York, 1970).
[36] M. A. Carpenter, in *Physical Properties and Thermodynamic Behaviour of Minerals*, edited by E. K. H. Salje (Reidel, Dordrecht, 1988), p. 265.
[37] E. K. H. Salje, B. Wruck, and H. Thomas, Z. Phys. B **82**, 399 (1991).
[38] E. K. H. Salje, B. Wruck, and S. Marais, Ferroelectrics **124**, 185 (1991).
[39] H.-W. Meyer, M. A. Carpenter, A. Graeme-Barber, P. Sondergeld, and W. Schranz, Eur. J. Mineral. **12**, 1139 (2000).
[40] H.-W. Meyer, S. Marion, P. Sondergeld, M. A. Carpenter, K. S. Knight, S. A. T. Redfern, and M. T. Dove, Am. Mineral. **86**, 566 (2001).
[41] P. Sondergeld, W. Schranz, A. V. Kityk, M. A. Carpenter, and E. Libowitzky, Phase Transit. **71**, 189 (2000).
[42] S. A. Hayward, S. A. T. Redfern, and E. K. H. Salje, J. Phys.: Condens. Matter **14**, 10131 (2002).
[43] M. A. Carpenter, H.-W. Meyer, P. Sondergeld, S. Marion, and K. S. Knight, Am. Mineral. **88**, 534 (2003).
[44] A. L. Goodwin, S. A. T. Redfern, M. T. Dove, D. A. Keen, and M. G. Tucker, Phys. Rev. B **76**, 174114 (2007).
[45] X. Qiu, Th. Proffen, J. F. Mitchell, and S. J. L. Billinge, Phys. Rev. Lett. **94**, 177203 (2005).

[46] V. Kiryukhin, T. Y. Koo, A. Borissov, Y. J. Kim, C. S. Nelson, J. P. Hill, D. Gibbs, and S.-W. Cheong, Phys. Rev. B **65**, 094421 (2002).
[47] D. N. Argyriou, U. Ruett, C. P. Adams, J. W. Lynn, and J. F. Mitchell, New J. Phys. **6**, 195 (2004).
[48] D. Saurel, A. Brulet, A. Heinemann, C. Martin, S. Mercone, and C. Simon, Phys. Rev. B **73**, 094438 (2006).
[49] C. Frontera and J. L. García-Munoz, Europhys. Lett. **84**, 67011 (2008).
[50] M. A. Carpenter, Am. Mineral. **92**, 328 (2007).
[51] J. M. Pérez-Mato and E. K. H. Salje, J. Phys.: Condens. Matter **12**, L29 (2000).
[52] T. Boffa Ballaran, M. A. Carpenter, M. C. Domeneghetti, E. K. H. Salje, and V. Tazzoli, Am. Mineral. **83**, 434 (1998).
[53] T. Boffa Ballaran, M. A. Carpenter, C. A. Geiger, and A. M. Koziol, Phys. Chem. Miner. **26**, 554 (1999).
[54] A. J. Atkinson, M. A. Carpenter, and E. K. H. Salje, Eur. J. Mineral. **11**, 7 (1999).
[55] E. K. H. Salje, M. A. Carpenter, T. Malcherek, and T. Boffa Ballaran, Eur. J. Mineral. **12**, 503 (2000).
[56] S. C. Tarantino, T. Boffa Ballaran, M. A. Carpenter, M. C. Domeneghetti, and V. Tazzoli, Eur. J. Mineral. **14**, 537 (2002).
[57] U. Rodehorst, M. A. Carpenter, T. Boffa Ballaran, and C. A. Geiger, Phys. Chem. Miner. **31**, 387 (2004).
[58] A. J. Millis, Solid State Commun. **126**, 3 (2003).